

# Fe doping effect of vanadium oxide films for enhanced switching electrochromic performances



Ju-Won Bae<sup>a,1</sup>, Bon-Ryul Koo<sup>b,1</sup>, Hyo-Jin Ahn<sup>a,b,\*</sup>

<sup>a</sup> Department of Materials Science and Engineering, Seoul National University of Science and Technology, Seoul 01811, Republic of Korea

<sup>b</sup> Program of Materials Science and Engineering, Convergence Institute of Biomedical Engineering and Biomaterials, Seoul National University of Science and Technology, Seoul 01811, Republic of Korea

## ARTICLE INFO

### Keywords:

Films  
Electrical properties  
Optical properties  
Transition metal oxides  
Electrochromic performances

## ABSTRACT

In the present study, Fe-doped  $V_2O_5$  films showing impressive electrochromic (EC) performance were developed using the sol-gel spin-coating method. To confirm the optimized Fe-doping effect on the  $V_2O_5$  films for the EC performance, we adjusted the Fe atomic percentages to 0.0, 0.5, 1.0, and 1.5 at%, respectively. With the effect of Fe doping on the  $V_2O_5$  films, the obtained films resulted in the formation of the oxygen vacancies. As the result, when the optimum Fe atomic percentage was 1.0 at%, the enhanced switching speeds (3.7 s for the bleaching speed and 2.0 s for the coloration speed) and enhanced coloration efficiency value ( $47.3 \text{ cm}^2/\text{C}$ ) compared to the other films were implemented. This can be attributed to the improved electrical conductivity and  $\text{Li}^+$  diffusion coefficient that led to efficient generation of the EC reaction activity and narrowing the optical bandgap at the coloration state to increase transmittance modulation. Therefore, this unique film can be a promising EC material to improve the performance for the EC devices.

## 1. Introduction

Due to the unique features such as reversible change of the optical properties, including color, reflection, and transmittance, under the behavior of voltage pulse, the electrochromic devices (ECDs) have received in enormous interest in terms of their use various applications, such as automobile sunroofs and mirrors, electronic displays, and smart windows [1,2]. Typical ECDs include the sandwich structure consisting of five functional layers: the electrolyte layer, two transparent conducting layers, and the cathodic electrochromic (EC) layer and the anodic EC layer [1–3]. For anodic EC layers, when a voltage is applied to the ECDs, the cationic species ( $\text{H}^+$  and  $\text{Li}^+$ ) inject into the EC layer to cause the bleaching of the devices. On the other hand, the ECDs become colored again by extracting the species from the EC layer, as the opposite voltage is applied to the devices [4,5]. Therefore, the EC layers are the most fundamental component in ECDs that profoundly dominates the EC performances in terms of transmittance modulation, coloration efficiency (CE), and switching speed. Among well-known EC materials are transition metal oxides such as tungsten oxide, vanadium oxide ( $V_2O_5$ ), titanium oxide, nickel oxide, and molybdenum oxide, all of which are characterized by good electrochemical stability, high

reliability, and low cost [5,6]. Among these,  $V_2O_5$  has attracted enormous interest as an exceptional EC material that can realize multi-color for the ECDs and can be employed as both their anodic and cathodic EC layers [7,8]. However, the practical applications of the  $V_2O_5$  on the ECDs are limited as compared to those of other metal oxides, as the  $V_2O_5$ -based films show low EC performances including narrow transmittance modulation, low coloration efficiency (CE), and slow switching speed originating from their low electrical conductivity and ion diffusion coefficient [7,9,10]. Therefore, considerable effort has been invested to enhancing the EC performances through elaborate modification of morphological, crystallographic, and electronic properties of the  $V_2O_5$ -based films [7–9,11,12]. In particular, the doping of metal ions into  $V_2O_5$  films is expected to improve the EC performances by varying valence vanadium state of  $V_2O_5$  which can enhance their electrical conductivity and ion diffusion coefficient [7,12]. For example, Panagopoulou et al. controlled the concentration of Mg doping on  $V_2O_5$  films using the RF magnetron reactive sputtering, reporting fast switching speeds (4.0 s for the bleaching speed and 10.0 s for the coloration speed) and wide transmittance modulation of 34.4% [12]. Furthermore, Lu et al. reported fabricating Ti-doped  $V_2O_5$  films using electrochemical deposition, resulting in that doping condition of 4 mol

\* Corresponding author at: Department of Materials Science and Engineering, Seoul National University of Science and Technology, Seoul 01811, Republic of Korea.

E-mail address: [hjahn@seoultech.ac.kr](mailto:hjahn@seoultech.ac.kr) (H.-J. Ahn).

<sup>1</sup> J.-W. Bae and B.-R. Koo contributed equally to this work.

<https://doi.org/10.1016/j.ceramint.2018.12.219>

Received 4 November 2018; Received in revised form 27 December 2018; Accepted 30 December 2018

Available online 31 December 2018

0272-8842/© 2019 Elsevier Ltd and Techna Group S.r.l. All rights reserved.

% Ti on the  $V_2O_5$  films exhibited optimized EC performances including the bleaching speed of 6.0 s, the coloration speed of 5.0 s, and transmittance modulation of 51.1% [7]. However, despite these enormous efforts, the research approach related to  $V_2O_5$  films doped with Fe element for high-performance ECDs has not been reported yet.

Therefore, in the present study, we fabricated Fe-doped  $V_2O_5$  films for high-performance ECDs using the facile sol-gel spin-coating method. Thereafter, we verified the optimized EC performances with the degree of Fe-doping on the  $V_2O_5$  films by proving the relationship between morphological and electronic properties and EC performances.

## 2. Experimental

Fe-doped  $V_2O_5$  films were fabricated using the sol-gel spin-coating method. First, the precursor solutions for spin coating were prepared by dissolving 0.1 M vanadium oxide ( $V_2O_5$ , Alfa Aesar) as a vanadium precursor and 10 wt% polyvinylpyrrolidone (PVP,  $M_w = 1,300,000$  g/mol, Aldrich) as an adhesion agent into de-ionized (DI) water with 5 vol % hydrogen peroxide ( $H_2O_2$ , Junsei), where the molar concentration of vanadium precursor was fixed as 0.1 M. Thereafter, iron (III) chloride hexahydrate as the doping agent was added to the above-prepared solution. In order to investigate the Fe-doping effect into the  $V_2O_5$ , we adjusted the atomic percentages of Fe to V to 0.0, 0.5, 1.0, and 1.5 at%. Then, the spin-coating of the solutions was performed on FTO glass substrates (Pilkington,  $8.0 \Omega/\square$ ) at 2000 rpm for 30 s. In the next step, all samples were annealed at  $500^\circ\text{C}$  for 1 h under air atmosphere, resulting in the formation of the Fe-doped  $V_2O_5$  films with varied Fe atomic percentages (thereafter referred to as bare  $V_2O_5$ , 0.5Fe- $V_2O_5$ , 1.0Fe- $V_2O_5$ , and 1.5Fe- $V_2O_5$ ).

The structural characterization of the resultant films was investigated using X-ray diffraction (XRD, Rigaku D/MAX2500V). The chemical binding state was analyzed using X-ray photoelectron spectroscopy (XPS, AXIS ultra-delay line detector equipped with an Al  $K_\alpha$  X-ray source, KBSI Daedeok Headquarters). The morphological properties were characterized using field-emission scanning electron microscopy (FE-SEM, Hitachi S-4800). The electrical and optical properties were measured by the hall-effect measurement (Ecopia, HMS-3000) and ultraviolet-visible (UV-vis) spectroscopy (Perkin-Elmer, Lambda-35), respectively. The electrochemical and EC performances were measured using a potentiostat/galvanostat (PGSTAT302N, FRA32M, Metrohm Autolab B.V., the Netherlands) in the 1 M  $LiClO_4$  electrolyte with a three-electrode electrochemical cell (Pt wire as the counter electrode, and Ag wire as the reference electrode). *In-situ* optical properties related to the switching speed and CE value were measured using ultraviolet-visible (UV-vis) spectroscopy (Perkin-Elmer, Lambda-35) in the wavelength of 415 nm.

## 3. Results and discussion

Fig. 1a shows the XRD patterns of the Fe-doped  $V_2O_5$  films formed with different Fe atomic percentages. Bare  $V_2O_5$  represents specific diffraction peaks at  $20.2^\circ$  and  $41.1^\circ$ , which correspond to the (001) and (002) planes of orthorhombic  $V_2O_5$  (JCPDS No. 89–0612), respectively. It can be clearly seen that the peak intensity of the (001) plane gradually decreased with an increase of the Fe atomic percentage from 0.0 to 1.0 at%, which can be related to the effect of Fe doping into  $V_2O_5$ . In addition, as another evidence of Fe doping, there is a peak shift of the (001) plane to lower  $2\theta$  value as the result of doping of  $Fe^{3+}$  with a relatively higher ion radius (0.64 Å) than that (0.54 Å) of  $V^{5+}$  for the  $V_2O_5$  (see Fig. 1b) [7]. Therefore, this doping can act as a major factor to vary their electronic properties due to the creation of oxygen vacancies along with the variation of V-O bond length by local mismatch of dopant with the matrix of cation charges [13]. However, for 1.5Fe- $V_2O_5$ , the decreased peak intensity and relaxed peak shift (as compared to that of 1.0Fe- $V_2O_5$ ) were observed, which may be due to the effect of the excessive Fe atomic percentages. This behavior was confirmed by the XPS results (see Fig. 2). All binding energies of the XPS spectra were calibrated by C 1 s (284.5 eV) as reference. In Fig. 2a, the V  $2p_{3/2}$  XPS spectra display two couple of characteristic peaks; one emitted at 516.9 eV which corresponds to  $V^{5+}$ ; the other peak emitted at 515.3 eV is related to  $V^{4+}$ , indicating the successful formation of the  $V_2O_5$  phases, as reported previously [14]. Interestingly, with an increase of the Fe atomic percentage, the area ratio of  $V^{4+}$  to  $V^{5+}$  increased from 12.05% for bare  $V_2O_5$  to 20.45% for 1.0Fe- $V_2O_5$ . This result can be attributed to an increase of the oxygen vacancies by the Fe doping into  $V_2O_5$  lattices, which matches well to the increased peaks related to the oxygen vacancies emitted at 529.4 eV of O 1 s (see Fig. 2b) [15]. However, 1.5Fe- $V_2O_5$  shows a decreased area ratio  $V^{4+}/V^{5+}$  (16.95%) compared to that of 1.0Fe- $V_2O_5$  in despite of high Fe atomic percentage, which is because of advent of Fe-O band related to  $Fe_2O_3$  phase, formed by a relatively excessive Fe atomic percentage (see O 1 s XPS spectra of Fig. 2b) [16].

Fig. 3 shows top-view SEM images obtained from bare  $V_2O_5$ , 0.5Fe- $V_2O_5$ , 1.0Fe- $V_2O_5$ , and 1.5Fe- $V_2O_5$ . Bare  $V_2O_5$  (see Fig. 3a) has the film structure crosslinked with the nanorods in the length range of 211.2–471.3 nm, in line with the accelerated (001) growth of the  $V_2O_5$  induced by the coordinating interaction of the PVP with vanadium precursors (see also the XRD results) [17]. With an increase of the Fe atomic percentage, the length of nanorods became shorter: from 189.6–401.1 nm for 0.5Fe- $V_2O_5$  (see Figs. 3b) to 169.9–340.9 nm for 1.5Fe- $V_2O_5$  (Fig. 3d). This could have been caused by the increased effect of the Fe doping on the  $V_2O_5$  to cause interference of crystal growth by distortion of the  $V_2O_5$  lattices [12]. Therefore, the XRD, XPS, and SEM results clearly demonstrate the successful formation of the Fe-

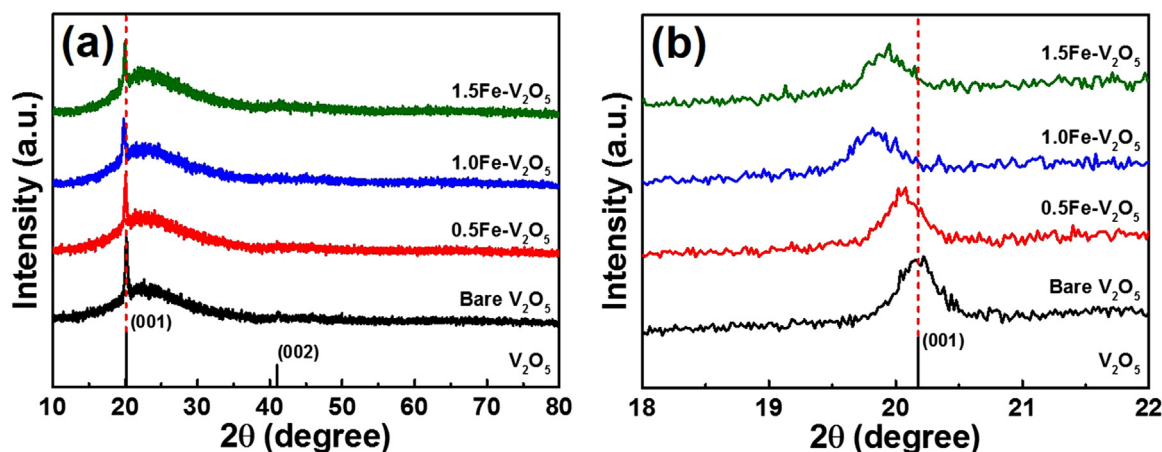


Fig. 1. (a) The XRD patterns and (b) magnified patterns in the range of  $18\text{--}22^\circ$  obtained from bare  $V_2O_5$ , 0.5Fe- $V_2O_5$ , 1.0Fe- $V_2O_5$ , and 1.5Fe- $V_2O_5$ , respectively.

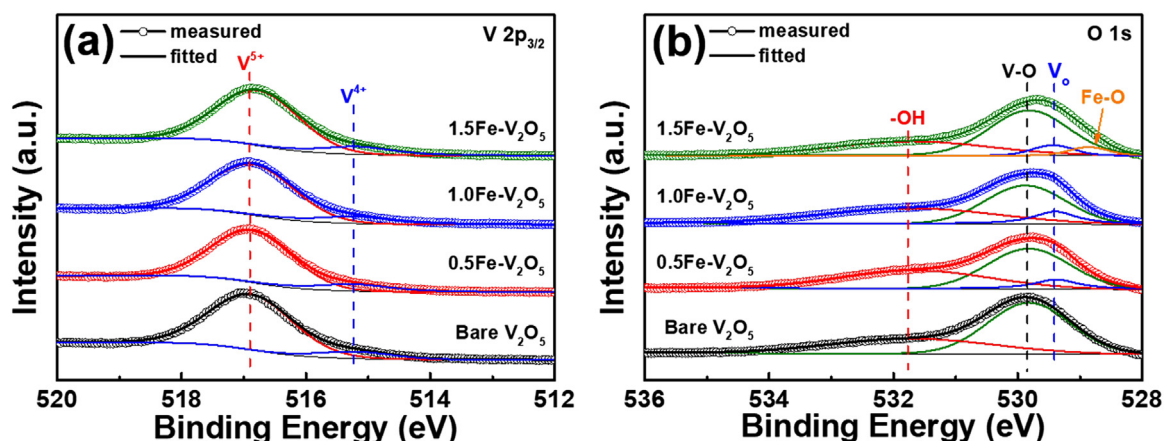


Fig. 2. The XPS spectra obtained from (a) V  $2p_{3/2}$  and (b) O  $1s$  for all films.

doped  $V_2O_5$  films and accurate adjustment of the degree of Fe doping on the  $V_2O_5$  films, which can lead to the improvement of the EC performance [18].

To confirm the variation of electrical properties with different Fe atomic percentage applied to the  $V_2O_5$  films, we measured the electrical conductivity of all films coated using a bare glass substrate (Corning EAGLE XG™). As shown in Fig. 4a, the value of the electrical conductivity gradually enhanced from bare  $V_2O_5$  ( $1.62 \times 10^{-7}$  S/cm) to  $1.0Fe-V_2O_5$  ( $2.75 \times 10^{-7}$  S/cm), and then declined when Fe atomic percentage was 1.5 at% ( $2.25 \times 10^{-7}$  S/cm). These results imply that  $1.0Fe-V_2O_5$  has a higher electrical conductivity than the other films owing to the improved effects of the oxygen vacancies by the optimized Fe doping on the  $V_2O_5$  that can efficiently transport the electrons and

$Li^+$  in the  $V_2O_5$  films [16]. In addition, as another effect of the Fe doping, variation of the optical band gap for the  $V_2O_5$  films was observed. This was revealed by calculating the relationship between the absorption coefficient ( $\alpha$ ) and the incident photon energy (see Eq. (1)) [19,20]:

$$(\alpha h\nu)^2 = D(h\nu - E_g)^n \quad (1)$$

where  $h$  is Planck's constant,  $\nu$  is photon frequency,  $D$  is a constant, and  $E_g$  is the optical band gap. The  $E_g$  values obtained by extrapolation of the linear region between  $(\alpha h\nu)^2$  and  $h\nu$  are 2.705 eV for bare  $V_2O_5$ , 2.688 eV for  $0.5Fe-V_2O_5$ , 2.661 eV for  $1.0Fe-V_2O_5$ , and 2.674 eV for  $1.5Fe-V_2O_5$ . The  $E_g$  narrowing from bare  $V_2O_5$  to  $1.0Fe-V_2O_5$  is due to the improved oxygen vacancies by increase of Fe doping to lift the

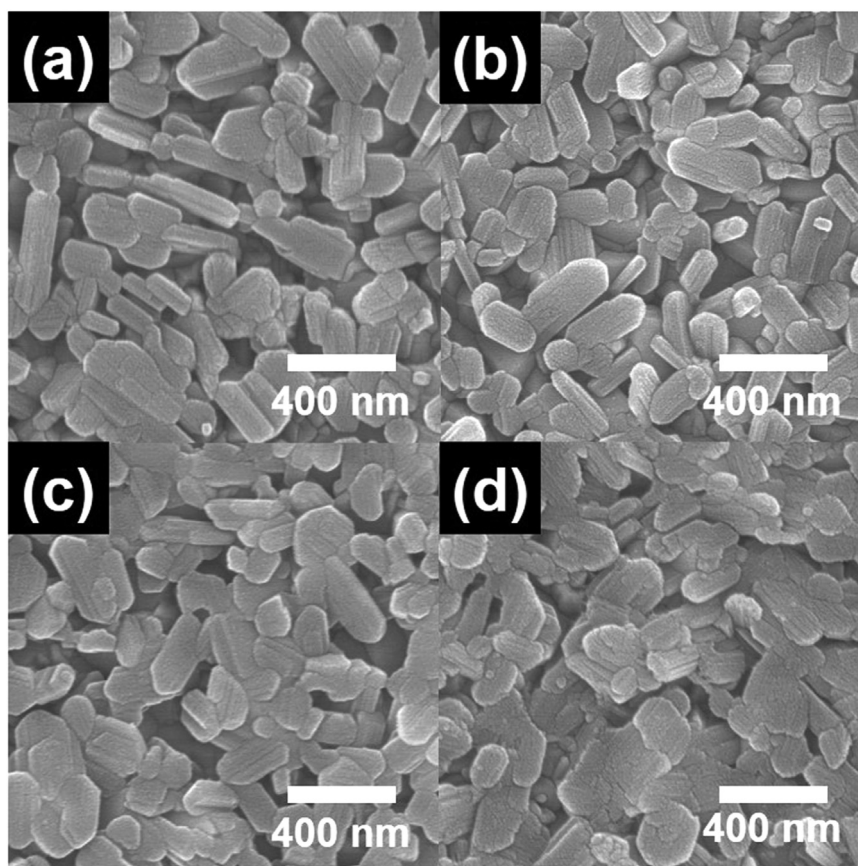


Fig. 3. Top-view FESEM images of (a) bare  $V_2O_5$ , (b)  $0.5Fe-V_2O_5$ , (c)  $1.0Fe-V_2O_5$ , and (d)  $1.5Fe-V_2O_5$ .

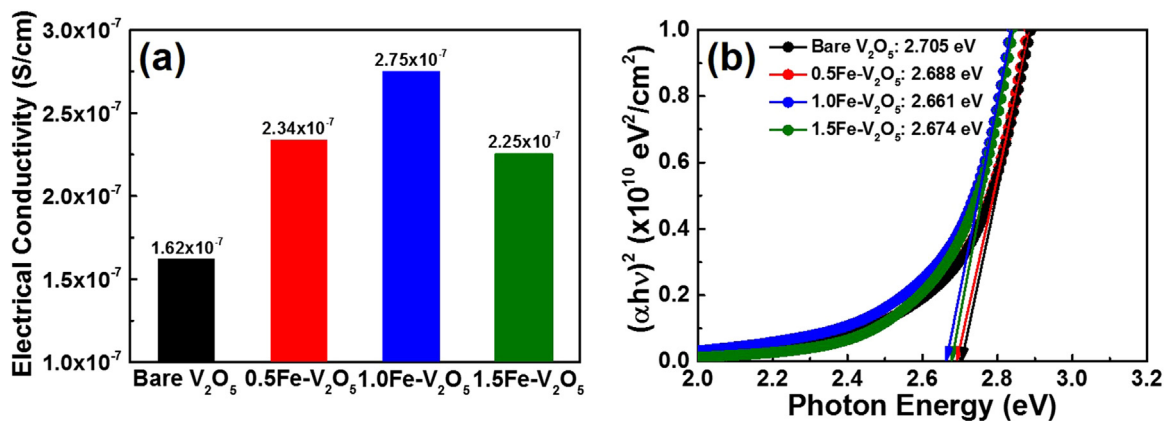


Fig. 4. (a) Electrical conductivities and (b) Tauc plots of bare V<sub>2</sub>O<sub>5</sub>, 0.5Fe-V<sub>2</sub>O<sub>5</sub>, 1.0Fe-V<sub>2</sub>O<sub>5</sub>, and 1.5Fe-V<sub>2</sub>O<sub>5</sub>.

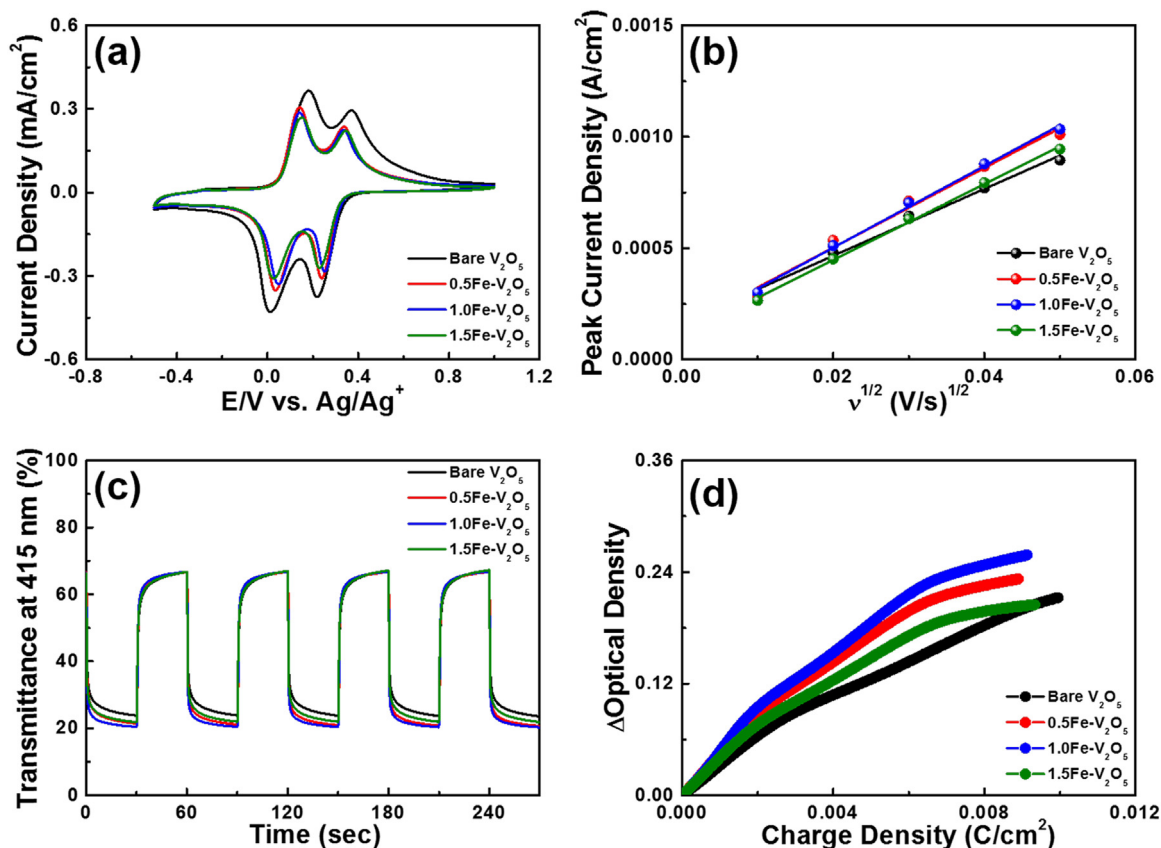


Fig. 5. (a) The CV curves measured in the potential range  $-0.5$ – $1.0$  V at the scan rate of  $20$  mV/s, (b) peak current density as a function of the square root of scan rate, (c) *in situ* optical transmittance at  $415$  nm with respect to the step potential applied at  $-0.5$  and  $1.0$  V for  $30$  s, and (d) OD variation with the extracted charge density for all films.

Table 1

Summary of the EC performance obtained from all films.

	T <sub>b</sub> (%)	T <sub>c</sub> (%)	Transmittance modulation (%)	Bleaching speed (s)	Coloration speed (s)	CE (cm <sup>2</sup> /C)
Bare V <sub>2</sub> O <sub>5</sub>	66.66	23.81	42.85	6.0	4.6	31.2
0.5Fe-V <sub>2</sub> O <sub>5</sub>	66.63	21.15	45.48	4.4	3.0	45.7
1.0Fe-V <sub>2</sub> O <sub>5</sub>	66.72	20.43	46.29	3.7	2.0	47.3
1.5Fe-V <sub>2</sub> O <sub>5</sub>	66.61	21.94	44.67	5.3	3.5	40.5

valance band of the V<sub>2</sub>O<sub>5</sub>, causing the absorption edge red shift to decrease the transparency of the V<sub>2</sub>O<sub>5</sub> films at the coloration state [21]. However, for 1.5Fe-V<sub>2</sub>O<sub>5</sub>, the E<sub>g</sub> value is observed to be improved as compared to that of 1.0Fe-V<sub>2</sub>O<sub>5</sub> despite high Fe atomic percentage,

which results from the formation of the Fe<sub>2</sub>O<sub>3</sub> phase confirmed from O 1 s XPS spectra (see Fig. 2c) [16]. Therefore, these results demonstrate that the electronic properties of the V<sub>2</sub>O<sub>5</sub> films were successfully adjusted with the effect of Fe doping that can directly affect the EC

performances including transmittance modulation, switching speed, and CE value.

To investigate the effect of Fe doping on electrochemical behavior of the  $V_2O_5$  films during the EC reaction, the CV measurements were performed in a three-electrode system with 1 M LiClO<sub>4</sub> as the electrolyte, Pt wire as the counter electrode, and Ag wire as the reference electrode in the potential range of  $-0.5$ – $1.0$  V at the scan rate of 20 mV/s (see Fig. 5a). In the case of the bare  $V_2O_5$ , the two well-defined reduction peaks centered at 0.21 and 0.01 V corresponding to the  $\alpha/\varepsilon$  and  $\varepsilon/\delta$  phase transitions, respectively, and the two well-defined oxidation peaks at 0.18 and 0.37 V corresponding to the  $\delta/\varepsilon$  and  $\varepsilon/\alpha$  phase transitions, respectively, were observed. This is indicative of multistep Li<sup>+</sup> intercalation/deintercalation processes of the typical orthorhombic  $V_2O_5$  (see the reaction in Eq. (2)) [22]:



As can be seen in the CV curve, with an increase of Fe atomic percentage, there were slight diminutions of the CV area originating from redox peaks of the samples due to distortion of the  $V_2O_5$ , as proved by the XRD peaks (see Fig. 1a). Interestingly, the potential separation with position of the reduction and oxidation peaks shifted to higher and lower potentials, respectively, gradually increasing from bare  $V_2O_5$  to 1.0Fe- $V_2O_5$ . This indicates the accelerated EC reaction activity in the films resulting from improved electrical conductivity. However, for 1.5Fe- $V_2O_5$ , there is a relaxation of the potential separation due to existence of the  $Fe_2O_3$  phase, leading to a decrease of the EC reaction activity [23]. This phenomenon is highly consistent with the results of Li<sup>+</sup> diffusion coefficient ( $D$ ) for the films, which can be obtained from the Randles–Sevcik equation (see Eq.(3)) [24]:

$$J_p = 2.72 \times 10^5 \times D^{1/2} \times C_o \times v^{1/2} \quad (3)$$

where  $J_p$  is the peak current density,  $C_o$  is the concentration of active ions in the solution, and  $v$  is the sweep rate. As shown in Fig. 5b, the obtained Li<sup>+</sup> diffusion coefficients were  $7.62 \times 10^{-10}$  cm<sup>2</sup>/s for bare  $V_2O_5$ ,  $10.80 \times 10^{-10}$  cm<sup>2</sup>/s for 0.5Fe- $V_2O_5$ ,  $11.36 \times 10^{-10}$  cm<sup>2</sup>/s for 1.0Fe- $V_2O_5$ , and  $9.78 \times 10^{-10}$  cm<sup>2</sup>/s for 1.5Fe- $V_2O_5$ . These results indicate that 1.0Fe- $V_2O_5$  has the highest Li<sup>+</sup> diffusion coefficient among those of the other samples (1.49 and 1.16 times in comparison with bare  $V_2O_5$  and 1.5Fe- $V_2O_5$ , respectively). Such high value of Li<sup>+</sup> diffusion coefficient for 1.0Fe- $V_2O_5$  can be ascribed to the improved oxygen vacancies resulting in an easy access to the EC reaction by optimized Fe-doping into  $V_2O_5$  films [18].

The investigation of the EC responses for the films was performed by tracing *in situ* transmittance at 415 nm by applying the step potentials of  $-0.5$  V (the bleached state) and 1.0 V (the colored state) to the devices for 30 s. From the obtained curves (see Fig. 5c), the transmittance modulation ( $\Delta T = T_b - T_c$ , where  $T_b$  and  $T_c$  are transmittances in the bleached and colored states, respectively) and the switching speed (defined as the time to reach 90% of the entire transmittance modulation at 415 nm) were determined (see Table 1 for a summary). Due to the decreased transmittance in the colored state by narrowing of the optical band gap as an effect of Fe doping into  $V_2O_5$ , the transmittance modulation increased from bare  $V_2O_5$  (42.85%) to 1.0Fe- $V_2O_5$  (46.29%). However, despite a relatively higher Fe atomic percentage, 1.5Fe- $V_2O_5$  reveals decreased transmittance modulation (44.67%) as compared to 1.0Fe- $V_2O_5$  due to the existence of the  $Fe_2O_3$  phases. In addition, for switching speeds, with an increase of the Fe atomic percentage, the accelerated values at 1.0Fe- $V_2O_5$  (3.7 s for the bleaching speed and 2.0 s for the coloration speed) was observed, which can be attributed to an improvement of the EC reaction activity as a result of the improved electrical conductivity and Li<sup>+</sup> diffusion coefficient by the optimized effect of Fe doping. Another important aspect for the EC application is the CE value, defined as the change in optical density ( $\Delta OD$ ) by the reacted charge per unit area ( $Q/A$ ). The CE value was calculated using Eq. (4) [2,24]:

$$CE = \frac{\Delta OD}{Q/A} = \left( \frac{A}{Q} \right) \log \left( \frac{T_b}{T_c} \right) \quad (4)$$

where  $Q$  and  $A$  are the integration of the current within the colored time and the given electrode area, respectively. That is, the desirable ECDs possess a high CE value due to ability of the large optical modulation with a low charge density. Fig. 5d shows the curves of the OD variation with respect to the extracted charge density at 415 nm. The obtained CE values were 31.2 cm<sup>2</sup>/C for bare  $V_2O_5$ , 45.7 cm<sup>2</sup>/C for 0.5Fe- $V_2O_5$ , 47.3 cm<sup>2</sup>/C for 1.0Fe- $V_2O_5$ , and 40.5 cm<sup>2</sup>/C for 1.5Fe- $V_2O_5$ . Therefore, 1.0Fe- $V_2O_5$  exhibited the highest CE value as compared to the other samples. This performance improvement was mainly due to the optimized Fe-doping into  $V_2O_5$ , leading to widening of the transmittance modulation (46.29%) caused from the decreased optical bandgap at the coloration state at the extracted charge density.

#### 4. Conclusion

In the present study, we successfully fabricated Fe-doped  $V_2O_5$  films to improve switching EC performances using the sol-gel spin-coating method by adjusting Fe atomic percentages (0, 0.5, 1.0, and 1.5 at%). As the effect of Fe doping into  $V_2O_5$ , the remarkable features forming oxygen vacancies on the films were observed, which resulted in an improvement of the EC reaction activity and narrowing of the optical bandgap on the films. As the result, the Fe-doped  $V_2O_5$  films fabricated with Fe 1.0 at% achieved the enhanced EC performance with the switching speeds and CE value. This performance improvement can mainly be attributed to optimized effects of Fe-doping into  $V_2O_5$  films; the noticeable fast switching speeds (3.7 s for the bleaching speed and 2.0 s for the coloration speed) were due to the increased EC reaction activity to improve the electrical conductivity and Li<sup>+</sup> diffusion coefficient; the high CE value (47.3 cm<sup>2</sup>/C) was related to a decreased optical bandgap at the coloration state to increase the transmittance modulation (46.29%) with respect to a small extracted charge density. Therefore, we contend that Fe doping on  $V_2O_5$  films can have a great potential for application as a high-performance EC material of the ECDs.

#### Acknowledgement

This study was supported by the Research Program funded by the SeoulTech (Seoul National University of Science and Technology)

#### References

- [1] W. Wu, M. Wang, J. Ma, Y. Cao, Y. Deng, Electrochromic metal oxides: recent progress and prospect, *Adv. Electron. Mater.* 4 (2018) 1800185.
- [2] B.-R. Koo, K.-H. Kim, H.-J. Ahn, Switching electrochromic performance improvement enabled by highly developed mesopores and oxygen vacancy defects of Fe-doped  $WO_3$  films, *Appl. Surf. Sci.* 453 (2018) 238–244.
- [3] K.-H. Kim, B.-R. Koo, H.-J. Ahn, Sheet resistance dependence of fluorine-doped tin oxide films for high performance electrochromic devices, *Ceram. Int.* 44 (2018) 9408–9413.
- [4] Z. Tong, Y. Tian, H. Zhang, X. Li, J. Ji, H. Qu, N. Li, J. Zhao, Y. Li, Recent advances in multifunctional electrochromic energy storage devices and photoelectrochromic devices, *Sci. China Chem.* 60 (2017) 13–37.
- [5] Z. Tong, S. Liu, X. Li, J. Zhao, Y. Li, Self-supported one-dimensional materials for enhanced electrochromism, *Nanoscale Horiz.* 3 (2018) 261–292.
- [6] M. Rakibuddin, H. Kim, Synthesis and characterization of facile industrially scalable and cost effective  $WO_3$  micro-nanostructures for electrochromic devices and photocatalyst, *Ceram. Int.* 44 (2018) 16615–16623.
- [7] Y. Lu, L. Liu, D. Mandler, P.S. Lee, High switching speed and coloration efficiency of titanium-doped vanadium oxide thin film electrochromic devices, *J. Mater. Chem. C* 1 (2013) 7380–7386.
- [8] R.S. de Oliveira, S.C. Oliveira, O.C. Alves, F.S. Semaan, E.A. Ponzio, Electrochromic behavior of vanadium oxide nanostructures synthesized by melt sonoquenching, *Rev. Virtual Quim.* 7 (2015) 1876–1892.
- [9] Z. Tong, X. Zhang, H. Lv, N. Li, H. Qu, J. Zhao, Y. Li, X.-Y. Liu, From amorphous macroporous film to 3D crystalline nanorod architecture: a new approach to obtain high-performance  $V_2O_5$  electrochromism, *Adv. Mater. Interfaces* 2 (2015) 1500230.
- [10] I. Pradeep, E.R. Kumar, N. Suriyanarayanan, Ch. Srinivas, M.V.K. Mehar, Effects of doping concentration on structural, morphological, optical and electrical properties

- of tungsten doped  $V_2O_5$  nanorods, *Ceram. Int.* 44 (2018) 7098–7109.
- [11] M. Liu, B. Su, Y. Tang, X. Jiang, A. Yu, Recent advances in nanostructured vanadium oxides and composites for energy conversion, *Adv. Energy Mater.* 7 (2017) 1700885.
- [12] M. Panagopoulou, D. Vernardou, E. Koudoumas, N. Katsarakis, D. Tsoukalas, Y.S. Raptis, Tunable properties of Mg-doped  $V_2O_5$  thin films for energy applications: li-ion batteries and electrochromics, *J. Phys. Chem. C* 121 (2017) 70–79.
- [13] R. Suresh, K. Giribabu, R. Manigandan, S. Munusamy, S. Praveen Kumar, S. Muthamizh, A. Stephen, V. Narayanan, Doping of Co into  $V_2O_5$  nanoparticles enhances photodegradation of methylene blue, *J. Alloy. Compd.* 598 (2014) 151–160.
- [14] C.-Y. Kim, A.A. Escudro, P.C. Stair, M.J. Bedzyk, Atomic-scale view of redox-induced reversible changes to a metal-oxide catalytic surface:  $vo_x/\alpha\text{-Fe}_2\text{O}_3(0001)$ , *J. Phys. Chem. C* 111 (2017) 1874–1877.
- [15] T. Yamashita, P. Hayes, Analysis of XPS spectra of  $Fe^{2+}$  and  $Fe^{3+}$  ions in oxide materials, *Appl. Surf. Sci.* 254 (2018) 2441–2449.
- [16] M. Caiado, A. Machado, R.N. Santos, I. Matos, I.M. Fonseca, A.M. Ramos, J. Vital, A.A. Valente, J.E. Castanheiro, Alkoxylation of camphene over silica-occluded tungstophosphoric acid, *Appl. Catal. A* 451 (2013) 36–42.
- [17] J.-J. Zhu, C.-X. Kan, J.-G. Wan, M. Han, G.-H. Wang, High-yield synthesis of uniform Ag nanowires with high aspect ratios by introducing the long-chain PVP in an improved polyol process, *J. Nanomater.* 2011 (2011) 1067–1076.
- [18] D.M. Yu, S.T. Zhang, D.W. Liu, X.Y. Zhou, S.H. Xie, Q.F. Zhang, Y.Y. Liu, G.Z. Cao, Effect of manganese doping on Li-ion intercalation properties of  $V_2O_5$  films, *J. Mater. Chem.* 20 (2010) 10841–10846.
- [19] S.T. Tan, B.J. Chen, X.W. Sun, W.J. Fan, H.S. Kwok, X.H. Zhang, S.J. Chua, Blueshift of optical band gap in ZnO thin films grown by metal-organic chemical-vapor deposition, *J. Appl. Phys.* 98 (2005) 013505.
- [20] S. Shaukat, M. Khaleeq-ur-Rahman, U. Ilyas, S. Naseem, I.M. Dildar, A. Latif, R.S. Rawat, Tailoring of optical band gap and electrical conductivity in a-axis oriented Ni doped Chromium Oxide thin films, *Ceram. Int.* 44 (2018) 11187–11195.
- [21] Y. Iida, Y. Kanno, Doping effect of M (M = Nb, Ce, Nd, Dy, Sm, Ag, and/or Na) on the growth of pulsed-laser deposited  $V_2O_5$  thin films, *J. Mater. Process. Technol.* 209 (2009) 2421–2427.
- [22] W. He, Y. Liu, Z. Wan, C. Jia, Electrodeposition of  $V_2O_5$  on  $TiO_2$  nanorod arrays and their electrochromic properties, *RCS Adv.* 6 (2016) 68997–69006.
- [23] Z. Li, C. Zhang, C. Liu, H. Fu, X. Nan, K. Wang, X. Li, W. Ma, X. Lu, G. Cao, Enhanced electrochemical properties of Sn-doped  $V_2O_5$  as a cathode material for lithium ion batteries, *Electrochem. Acta* 222 (2016) 1831–1838.
- [24] B.-R. Koo, H.-J. Ahn, Fast-switching electrochromic properties of mesoporous  $WO_3$  films with oxygen vacancy defects, *Nanoscale* 9 (2017) 17788–17793.